Chemical Engineering Science 199 (2019) 164–178

Contents lists available at ScienceDirect

Chemical Engineering Science

journal homepage: www.elsevier.com/locate/ces

Integrated control and process design for improved load changes in fluidized bed boiler steam path

Matias Hultgren *, Enso Ikonen, Jenő Kovács

Systems Engineering, University of Oulu, Linnanmaa, POB 4300, FI-90014 Oulun yliopisto, Finland

HIGHLIGHTS

- Process and control design were integrated for a fluidized bed boiler steam path.
- The steam storage distribution and feedback controllers were optimized together.
- Boiler-following control was assessed and selected based on relative gain methods.
- Improved load transitions, controllability and disturbance rejection were reached.
- The design suggested a large total steam storage, preferably close to the turbine.

GRAPHICAL ABSTRACT

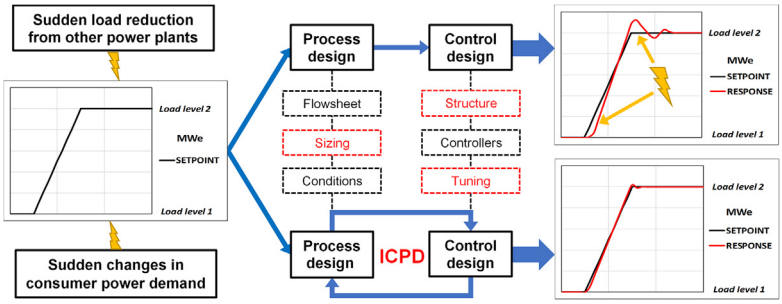

ARTICLE INFO

Article history:
Received 27 June 2018
Received in revised form 21 November 2018
Accepted 5 January 2019
Available online 23 January 2019

Keywords:
Integrated control and process design
Power plant control
Process optimization
Performance relative gain array
Closed-loop disturbance gain
Plant-wide control

ABSTRACT

Integrated control and process design is considered for a power plant to obtain improved load changes in output electrical power (MW_e). Fast load transitions are increasingly needed in conventional power plants, which calls for a deeper integration between the boiler and its control system. An integrated design methodology is applied to an industrial boiler steam path in this paper; no past reports of such an application exist in the literature. The methodology utilizes dynamic optimization together with performance relative gain array and closed-loop disturbance gain controllability analysis. The aim is to optimize the boiler steam storage distribution, the turbine valve operation, and the electrical power and main steam pressure controllers during different MW_e ramp reference trajectories. The methodology was successful in defining closed-loop designs with excellent MW_e setpoint tracking, small steam pressure disturbances and minimal steam throttling. The results also highlighted the challenges related to integrated design in power plants.

1. Introduction

In this paper, integrated control and process design is performed for a circulating fluidized bed (CFB) boiler. Dynamics and control are becoming increasingly important in the operation of thermal power plants due to demands from the power generation market (IEA, 2011). Most importantly, combustion power plants are increasingly operated in fast load transitions (Alobaid et al., 2016; Franzosi et al., 2006; Kovács et al., 2012; Wang et al., 2014) and less at maximum load with the best operational efficiency. Improving the load change performance is challenging due to the complex dynamics and interconnected nature of the boiler steam cycle. Increased emission requirements, challenging

* Corresponding author at: Outotec, Kuparitie 10, PO Box 69, FI-28101 Pori, Finland.
E-mail addresses: hultgrenmatias@gmail.com, matias.hultgren@outotec.com (M. Hultgren), Enso.Ikonen@oulu.fi (E. Ikonen), Jeno.Kovacs@oulu.fi (J. Kovács).

https://doi.org/10.1016/j.ces.2019.01.025
0009-2509/

Nomenclature

CFB	circulating fluidized bed
CV	controlled output variable
e_E	mass flow to turbine electrical power conversion factor, MW·s·kg^{-1}
d	process disturbance variable, –
DSH	desuperheater spray
D_p	derivative gain for pressure "p" PID controller, –
E	output electrical power at the turbine, MW
F	frequency range for relative gain analysis, rad/s
f	pipe friction factor, 1/m^4
$\mathbf{G}$	open-loop process transfer function matrix between CVs and MVs
$\bar{\mathbf{G}}$	scaled open-loop process transfer function matrix
$\hat{\mathbf{G}}$	diagonal matrix of the control MV–CV connections
g	gain magnitude between CV and MV, –
$\mathbf{G}_d$	open-loop disturbance transfer function matrix between CVs and disturbances
$\bar{\mathbf{G}}_d$	scaled open-loop disturbance transfer function matrix
$\hat{\mathbf{G}}_d$	closed-loop disturbance gain (CLDG) matrix in the frequency domain
$\mathbf{I}$	identity matrix
I_i	integral gain for output "i" PID controller ("p" or "E"), –
ICPD	integrated control and process design
J	integrated control and process design objective function, –
j	individual design objective, –
m_W	steam mass flow, subscripts "in" and "out" for input and output, kg/s
$\bar{m}_W$	nominal steam mass flow, kg/s
L	firing power, kg/s
MV	manipulated input variable
N_p	derivative filter for pressure "p" PID controller, –
p	main steam pressure, bar
p_i	steam pressure in a section "i", subscript "n" denotes pressure after the section, bar
$\bar{p}$	nominal steam pressure, bar
P_i	proportional gain for output "i" PID controller ("p" or "E"), –
q_E	evaporator storage percentage parameter, %
q_{S1}	parameter for percentage of superheater storage before DSH cooling, %
r	valve coefficient, m·s
RGA	relative gain array
SP	setpoint
s	Laplace s-plane operator, rad/s
T	time range of dynamic testing, s
t	time, s
t_I	boiler thermal inertia time delay, s
u	process input variable, subscript "c" denotes control of a specific output, –
v	turbine valve position, –
$\bar{v}$	nominal turbine valve position, –
x_{HP}	portion of the electrical power that is generated at the turbine high-pressure section, –
y	process output variable, –
$\mathbf{\Gamma}$	performance relative gain array (PRGA) matrix in the frequency domain, –
Γ_n	PRGA number in the frequency domain, –
ρ_W	steam density, kg/m^3
τ_E	evaporator steam storage coefficient, m·s^2
τ_S	superheater (SH) steam storage coefficient, m·s^2
τ_{S1}	superheater steam storage coefficient before DSH spray cooling, m·s^2
τ_{S2}	superheater steam storage coefficient after DSH spray cooling, m·s^2
τ_{HP}	turbine high-pressure section time constant, s
τ_I	boiler thermal inertia time constant, s
τ_{LP}	turbine low-pressure section time constant, s
τ_{TOT}	normalized total steam storage parameter, m·s^2
ω	radial frequency, rad/s

new fuels and new technologies like oxy-firing introduce additional challenges for boiler operation.

The new requirements call for advanced control and effective control design methods. Centralized model predictive control (MPC) has been a major driving force in this work (Aurora et al., 2004; Chan et al., 2014; Franzosi et al., 2006; Klaučo and Kvasnica, 2017; Ławryńczuk, 2017; Prasad et al., 2000; Prasad et al., 2002; Rovnak and Corlis, 1991). The application of fuzzy and neural network MPC has been frequently reported for increasing the coordination between the boiler and the turbine, and for overcoming problems due to complex process dynamics (Kong et al., 2015; Liu et al., 2010; Ma et al., 2016; Zhang et al., 2017). In general, a plantwide design focus is essential for achieving an improved coordination of the power plant control tasks. Systematic plantwide control has mainly been deployed for specific boiler setups, such as oxy combustion (e.g. Niva et al., 2015; Niva et al., 2017; Jin et al., 2015). Hultgren et al. (2015, 2017b) examined plantwide control structure selection and interaction analysis based on relative gains for once-through and oxy-fired CFB boilers. Multiloop PID decoupling and tuning was investigated e.g. by Garduno-Ramirez and Lee (2005), Garrido et al. (2009) and Zhang et al. (2012). Moreover, established operational methods like condensate throttling (Long et al., 2017; Wang et al., 2017), steam extraction setups at the turbine (Kovács et al., 2012; Zhou and Wang, 2017), and condenser control adjustments (Wang et al., 2014; Wang et al., 2015) are still being investigated in order to reach improved performance.

Despite advances in load transition control, control design alone is not going to be enough to meet the performance challenges in thermal boiler design, as the restrictions to setpoint tracking and stability are ultimately determined by the process design. A deeper interaction between process and control design is needed to obtain improved output power responses, high efficiency, sufficient steam quality and good operational safety. In integrated control and process design (ICPD), the process and its control system are designed at the same time (Sharifzadeh, 2013; Vega et al., 2014), which enables the consideration of dynamic bottlenecks that limit achievable control performance. At the same time, process specific dynamics can be incorporated more thoroughly into the boiler control system design.

Integrated design can be carried out using a process knowledge oriented approach, or the problem can be formulated as a "closed" framework, where process and control parameters are optimized (Hultgren et al., 2017a). This paper investigates ICPD optimization (Sakizlis et al., 2004; Yuan et al., 2012) for conventional power plant load change performance. The optimization formulation depends on the design scope and current status (greenfield or existing plant) of the target boiler (Fig. 1).

This paper considers fully simultaneous ICPD design for the steam path of an industrial-scale CFB drum boiler. The aim is to

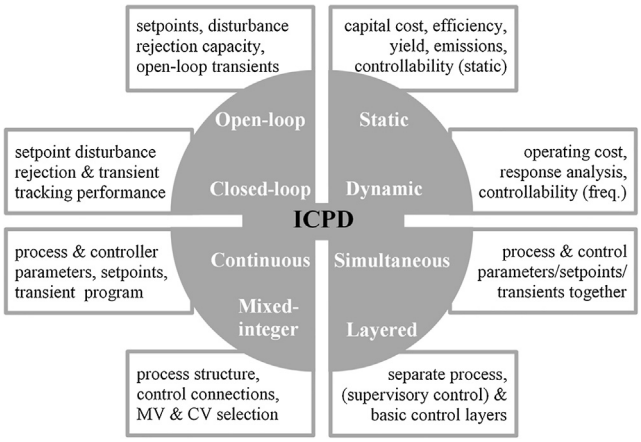

Fig. 1. Algorithm structures and features of ICPD optimization. Design applications and variables are listed in the accompanying text boxes. MV/CV = manipulated/controlled variable, freq. = frequency.

determine how the steam storage capacity should be distributed in the boiler, and how the main control loops should be tuned to obtain faster load changes. Sufficient controllability should also be maintained in the steam path, measured with the performance relative gain (PRGA) and closed-loop disturbance gain (CLDG) arrays. The evaporator and superheater steam storage capacities, the turbine valve nominal position, and the main steam pressure and electrical power PID controller parameters are optimized using a systematic ICPD design methodology. The main contribution of the paper is to propose a method for deriving power plant steam cycle design guidelines and to demonstrate the benefits of an integrated ICPD approach for thermal power plants.

Currently there is little existing literature available concerning ICPD in combustion power plants. Diangelakis et al. utilized mixed-integer dynamic optimization for residential scale power plants (Diangelakis et al., 2017; Diangelakis and Pistikopoulos, 2016; Diangelakis and Pistikopoulos, 2017). Capra and Martelli (2015) carried out a joint process and part-load design for organic Rankine cycles, using continuous derivative-free optimization. Chen and Bollas (2017) optimized air preheating and steam temperature setpoints together with supervisory control for a chemical looping plant. Hultgren et al. (2017a) made a literature review about ICPD design in power plants, and specified possibilities for applying ICPD in CFB boilers. The work contained basic ICPD design examples for a CFB steam path, and in the present paper these initial simulations are extended into a full ICPD design case.

The paper is structured as follows. Section 2 outlines the operational principle of the CFB boiler and its steam cycle. Section 3 presents the storage capacity model that is used for investigating boiler load changes and discusses the relative gain design tools and optimization methods that are utilized in the ICPD framework. Section 4 presents the CFB steam path ICPD design setup, followed by assessment of the performance of the design via simulations in Section 5. Finally, Section 6 concludes the paper.

2. Boiler process and control

The combustion power plant is divided into the combustion side and water-steam cycle subsystems (Alobaid et al., 2016; Joronen et al., 2007; Sarkar, 2015). Fuel is combusted in the furnace, and heat is transferred to the water-steam side. Feedwater is pumped and evaporated in the furnace evaporator, and the saturated steam is heated further in the superheating block, which often consists of several superheater (SH) units and cooling desuperheater spray flows (DSH). The formed main steam expands stage-wise in the turbine (high-pressure and low-pressure sections) to generate power.

Depending on the evaporator setup, boilers are classified into drum or once-through boilers. In drum boilers, water and steam are separated in a drum after the evaporation and recirculated to the evaporator. In once-through boilers, evaporation and superheating take place in a once-through path with no set separation stage. Another defining feature of the boiler is whether it is used in constant- or sliding-pressure mode. In constant-pressure mode, a constant main steam pressure is maintained at the turbine on different boiler load levels. While this enables the use of stored steam as a fast control reserve on part-loads, throttling the steam flow with the turbine valve contributes heavily to exergy destruction and leads to reduced operational efficiency. In sliding-pressure mode, the main steam pressure is altered together with the boiler load level, which enables a high efficiency. However, when operating in pure sliding mode with the turbine valve fully open, no fast steam control reserves can be utilized for load changes.

The main controlled parameters of a condensing power plant (Joronen et al., 2007; Klefenz, 1986) are the generated power and the main steam properties, i.e. flow, temperature and pressure (Fig. 2). The output electrical power (MW_e) is controlled either with the fuel firing power or by modifying the steam flow to the turbine with the turbine throttling valve. The main steam pressure can similarly be modified either with the turbine valve or the firing power, which is regulated by combustion control. Feedwater is controlled to provide enough water for steam formation. The main steam temperature is typically adjusted with the DSH sprays in the superheating section.

Electrical power and main steam pressure control is coordinated with the unit master strategy (Fig. 2), the basic setups of which are boiler-following and turbine-following control (Joronen et al., 2007). In boiler-following control, the electrical power is controlled with the turbine valve and the pressure with the fuel firing power. The MW_e setpoint alters the steam flow, and the pressure disturbance is compensated with the firing power. In turbine-following control, the opposite connections are applied: The firing power is altered according to the MW_e setpoint, and the turbine valve position is changed to regulate the pressure.

Proper selection of the unit master control strategy is crucial for improving load change performance. Altering the steam flow to the turbine with the turbine valve results in immediate changes in the MW_e output, which enables fast and accurate load changes. However, this only provides a transient response to the electrical power, as the generated steam from the evaporation remains unchanged. Controlling the MW_e output with the firing power is slow, but at steady-state the generated steam and thus the electrical power mainly depend on the firing power. These effects can be observed from Fig. A1, where the electrical power was controlled with the fuel + air flows or the turbine valve only. When the constraints of the manipulated variables were disregarded, the turbine valve opening had to be increased constantly to maintain the new electrical power setpoint, while using the fuel + air flows for MW_e control slowly settled on a new steady-state. On the other hand, tight control was easily achieved during the ramp with the turbine valve, whereas the combustion power required almost instantaneous, practically infeasible changes in order to achieve a comparable MW_e response.

The target process of this paper is the steam path of an industrial condensing drum boiler in the range of >100 MW_e with steam superheating and a two-stage turbine expansion. The power plant uses the CFB combustion technology, where fuel and bed material particles are fluidized with the oxidant gas flows and circulated in the furnace hotloop (Kovács et al., 2012; Sarkar, 2015). The dynamic behavior of the combustion side is simplified as a thermal inertia term.

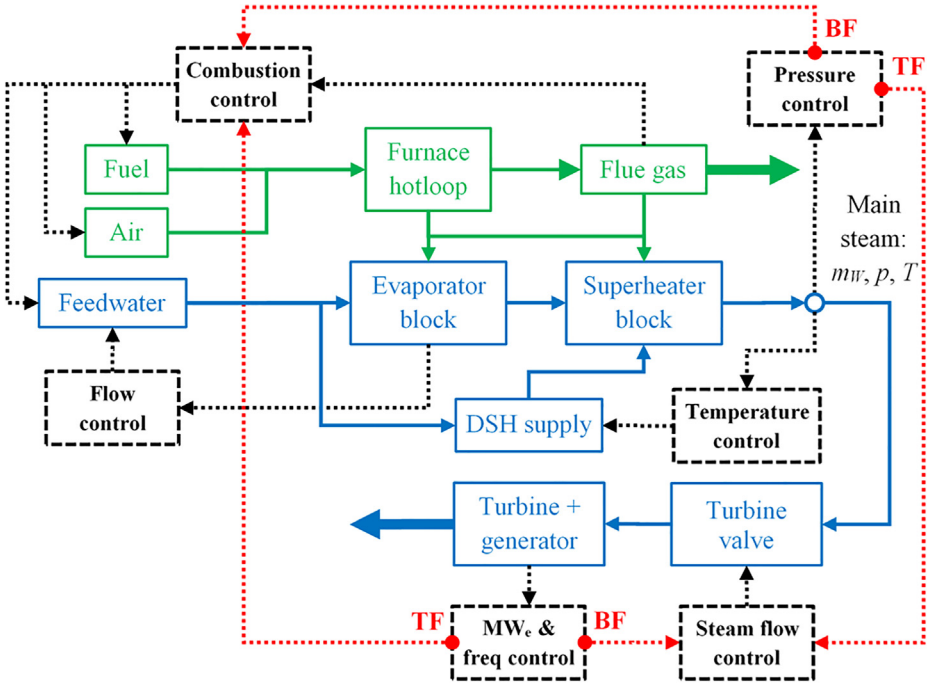

Fig. 2. Control of main steam properties and output MW_e, schematic figure. Dashed lines are control connections, boiler-following (BF) and turbine-following (TF) control schemes are highlighted.

3. Model and methods

The modeling and design tools of this paper are described here. Section 3.1 describes the boiler model, Section 3.2 the controllability analysis tools, and Section 3.3 the ICPD optimization. The goal of the ICPD design was to optimize the steam storages and electrical power/steam pressure controllers to obtain accurate MW_e set-point tracking, small steam pressure disturbances and good controllability. The ICPD modeling aimed at describing the process as a series of interconnected dynamic elements, where the effect of design parameters could be separated from the overall input–output responses. The individual process stages were thus modeled using simple linear dynamics, which together resulted in a higher-order transfer function matrix in the Laplace "s" domain. This approach is admissible in the region surrounding the nominal operating point, when considering the steam path mass storage dynamics.

3.1. Steam path model

The industrial power plant model is a generic dynamic steam path model that is used at the Sumitomo SHI FW company for load transition control design. It consists of transfer function elements for the boiler, evaporator, superheater, turbine and turbine valve. The model describes the relation between steam pressure and flow at different stages of the steam path, as well as the relation to the output electrical power at the turbine (Doležal and Varcop, 1970).

The evaporation and superheating sections are considered as lumped mass storages for steam, i.e. "mass storage coefficients" τ_E and τ_S, Eq. (1), which translate into time constants. The superheating storage coefficient is divided into two terms (τ_{S1} and τ_{S2}) in order to investigate DSH spray disturbances. The driving force for the steam flow is the pressure difference over the section, Eq. (2).

$$p_i(s) = \frac{1}{C \cdot s}\left[m_{W,in}(s) - m_{W,out}(s)\right] \tag{1}$$

$$p_i(s) - p_{i,n}(s) = \frac{2 \cdot f \cdot \bar{m}_{W,out}}{\rho_W} m_{W,out}(s) \tag{2}$$

where C is the mass storage coefficient of the evaporator (τ_E) or superheater (τ_S), p_i is steam pressure in section "i", $p_{i,n}$ is steam pressure after section "i", $m_{W,in}$ and $m_{W,out}$ are input and output steam mass flows ($\bar{m}_{W,out}$ is nominal flow), ρ_W is steam density, and f is a pipe friction factor that depends on the pressure and load levels in the boiler.

The thermal inertia of the boiler is a first-order block (3) that describes the steam generation dynamics between the combustion side input flows (fuel and air) and the formed steam on the water-steam side.

$$\frac{m_{W,out}(s)}{L(s)} = e^{-t_l \cdot s}\frac{1}{\tau_l \cdot s + 1} \tag{3}$$

where τ_l is thermal inertia, t_l is load change delay and L is firing power (combustion side load).

The turbine is modeled using first-order transfer functions (4) that describe the dynamics between the incoming steam and the generated power (Joronen et al., 2007; Kundur, 1994). The turbine consists of a high-pressure and low-pressure section. The turbine valve is modeled as the product of the main steam pressure, the valve position and a valve coefficient "r", linearizing the bilinear term in Eq. (5).

$$\frac{E(s)}{m_{W,in}(s)} = e_E\left(\frac{x_{HP}}{\tau_{HP} \cdot s + 1} + \frac{1 - x_{HP}}{\tau_{LP} \cdot s + 1}\right) \tag{4}$$

$$m_{W,out}(s) = rp(s)v(s) = r\bar{p}v(s) + r\bar{v}p(s) \tag{5}$$

where x_{HP} is the portion of power generated in the high-pressure turbine, τ_{HP} and τ_{LP} are high- and low-pressure turbine time constants, E is electrical power, e_E is a conversion factor, r is valve coefficient, and v is turbine valve position; $\bar{p}$ and $\bar{v}$ are nominal pressure and valve position values.

The steam path model can be constructed from Eqs. (1)–(5) according to Fig. A.2, Appendix A. The nominal model parameters

are obtained from steam tables and in-house design data. Linearizing, an open-loop 2×2 transfer function matrix (6) between the investigated inputs and outputs of the boiler can be constructed. The manipulated variables (MV) are the firing power L and the turbine valve position v. The controlled variables (CV) are the main steam pressure p and electrical megawatts E.

$$\mathbf{G}(s) = \begin{bmatrix} \frac{p(s)}{L(s)} & \frac{p(s)}{v(s)} \\ \frac{E(s)}{L(s)} & \frac{E(s)}{v(s)} \end{bmatrix} = \begin{bmatrix} e^{-t_l \cdot s} \frac{\alpha_{11}}{s^4+\beta_{11} \cdot s^3+\gamma_{11} \cdot s^2+\delta_{11} \cdot s+\varepsilon_{11}} & \frac{-\alpha_{12} \cdot s^2-\beta_{12} \cdot s-\gamma_{12}}{s^3+\delta_{12} \cdot s^2+\varepsilon_{12} \cdot s+\zeta_{12}} \\ e^{-t_l \cdot s} \frac{\alpha_{21} \cdot s+\beta_{21}}{s^6+\gamma_{21} \cdot s^5+\delta_{21} \cdot s^4+\varepsilon_{21} \cdot s^3+\zeta_{21} \cdot s^2+\eta_{21} \cdot s+\theta_{21}} & \frac{\alpha_{22} \cdot s^4+\beta_{22} \cdot s^3+\gamma_{22} \cdot s^2+\delta_{22} \cdot s}{s^5+\varepsilon_{22} \cdot s^4+\zeta_{22} \cdot s^3+\eta_{22} \cdot s^2+\theta_{22} \cdot s+\kappa_{22}} \end{bmatrix} \tag{6}$$

where $\mathbf{G}$ is the input-output process transfer function matrix, and α, β, γ, δ, ε, ζ, η, θ, κ are positive coefficients provided in Eqs. (B.1)–(B.4), Appendix B.

The main steam temperature is assumed to be perfectly controlled with a DSH spray between superheater storages τ_{S1} and τ_{S2}. This means that active steam temperature control with the DSH flow will generate steam mass flow disturbances to superheating section 2 at a specified operating point, while superheating section 1 will be unaffected by these disturbances. The DSH spray disturbance transfer function is derived as Eq. (7) from the block diagram in Fig. A.2.

$$\mathbf{G}_d(s) = \begin{bmatrix} \frac{p(s)}{d(s)} \\ \frac{E(s)}{d(s)} \end{bmatrix} = \begin{bmatrix} \frac{\alpha_{d1} \cdot s^2+\beta_{d1} \cdot s+\gamma_{d1}}{s^3+\delta_{d1} \cdot s^2+\varepsilon_{d1} \cdot s+\zeta_{d1}} \\ \frac{\alpha_{d2} \cdot s^3+\beta_{d2} \cdot s^2+\gamma_{d2} \cdot s+\delta_{d2}}{s^5+\varepsilon_{d2} \cdot s^4+\zeta_{d2} \cdot s^3+\eta_{d2} \cdot s^2+\theta_{d2} \cdot s+\kappa_{d2}} \end{bmatrix} \tag{7}$$

where d is a disturbance, $\mathbf{G}_d$ is the disturbance transfer function matrix between p and E and the DSH spray disturbance d, and α_d, β_d, γ_d, δ_d, ε_d, ζ_d, η_d, θ_d, κ_d are positive coefficients provided in Appendix B, Eqs. (B.5)–(B.6).

In total, the overall 2×2 steam path model can be illustrated in Fig. 3. The figure also shows how p and E can be controlled by L and v through unit master control.

3.2. Controllability & interaction analysis

The boiler control structure is selected based on the performance relative gain array (PRGA) and the closed-loop disturbance gain (CLDG). Controllability often refers to "state controllability" in control theory and is evaluated e.g. by considering the controllability matrix rank (Kalman criterion). In this paper, the "input–output controllability" definition is used, as it is relevant for industrial control design (Skogestad and Postlethwaite, 2005). Input–output controllability ensures that outputs can be kept within a set band from their references despite unknown bounded variations (disturbances or process changes), and it can be analyzed e.g. with relative gain methods like the PRGA and CLDG.

The PRGA and CLDG are based on the relative gain array (RGA) (Bristol, 1966), modified for the frequency domain (Witcher and McAvoy, 1977; McAvoy, 1983). The RGA consists of input–output interaction measures that signify how process open-loop gains change when other loops are closed (Ogunnaike and Ray, 1994). Control connections with elements close to 1 are ideal; negative values result in a gain sign change and should be avoided; small positive values result in gain amplification when loops are closed; and large elements signify gain amplification when loops are opened.

The PRGA is calculated as a scaled inverse of the plant at zero frequency (gains) or higher frequencies (frequency responses). A general definition for a 2×2 MV–CV system PRGA is shown in Eq. (8).

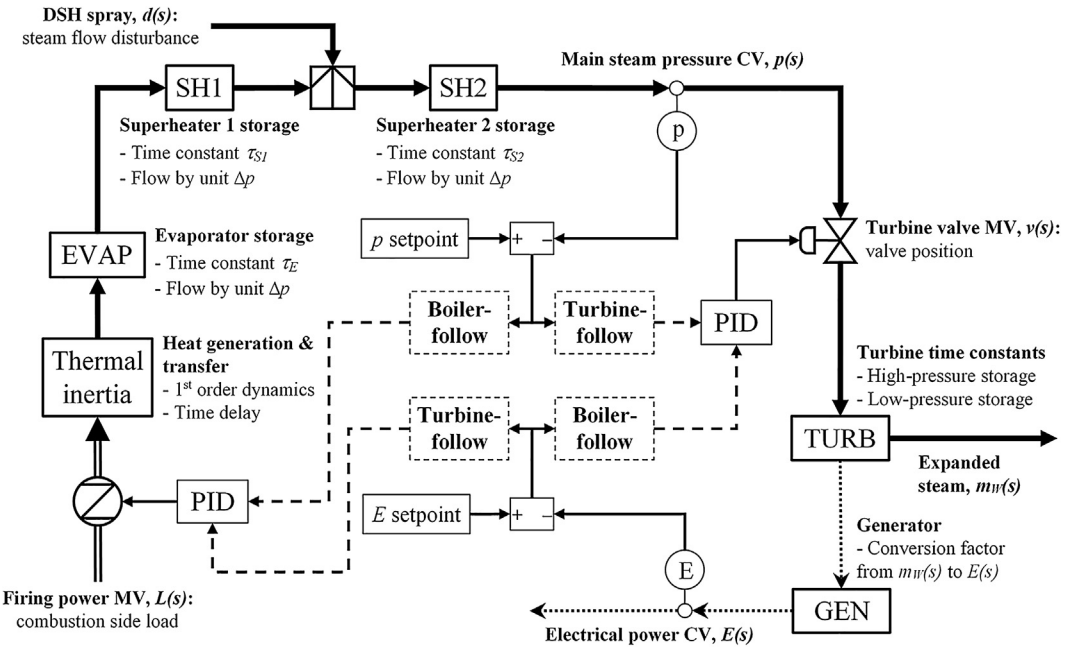

Fig. 3. Conceptual diagram of the process model between MVs and CVs. The alternative boiler-following and turbine-following unit master control connections are illustrated.

$$\mathbf{\Gamma}(s) = \hat{\mathbf{G}}(s) \cdot \bar{\mathbf{G}}(s)^{-1} = \begin{bmatrix} \frac{y_1(s)}{u_{c1}(s)} & 0 \\ 0 & \frac{y_2(s)}{u_{c2}(s)} \end{bmatrix} \cdot \begin{bmatrix} \frac{y_1(s)}{u_1(s)} & \frac{y_1(s)}{u_2(s)} \\ \frac{y_2(s)}{u_1(s)} & \frac{y_2(s)}{u_2(s)} \end{bmatrix}^{-1} \quad (8)$$

where $\mathbf{\Gamma}$ is the PRGA, $\hat{\mathbf{G}}$ is a scaled diagonal transfer function matrix of the control MV–CV connections, $\bar{\mathbf{G}}$ is a scaled process transfer function matrix, u denotes scaled input MVs (L and v), y denotes scaled output CVs (p and E), and u_{cn} is the input used for controlling output "n".

Among the relative gain methods, the PRGA is well-suited for highlighting controllability related feedback control limitations for the MV–CV connections of a chosen control system. Diagonal PRGA elements are the same as in the RGA and should ideally be close to 1. Off-diagonal elements signify interactions that have a detrimental effect on control performance and should be as small as possible. Control structures can conveniently be ranked in a specified frequency range ω with the PRGA number, Eq. (9), comparing the PRGA to the ideal case, i.e. an identity matrix $\mathbf{I}$.

$$\Gamma_n(s) = \|\mathbf{\Gamma}(s) - \mathbf{I}\|_N \quad (9)$$

where Γ_n is the PRGA number and N denotes a chosen norm. The absolute sum norm is used in this paper, similarly to Skogestad and Postlethwaite (2005). Notably, the PRGA is more applicable for examining one-way interactions than the basic RGA, which always gives an identity matrix for a triangular process system. This feature is especially useful for the negligible steady-state electrical power gain of the turbine valve (c.f. Section 2), which is also visible in the process model equations, as the $E(s)/v(s)$ transfer function has a zero in the origin in Eq. (6).

The DSH spray flow effects are analyzed at different frequencies with the CLDG, general definition for a 2×2 MV–CV system with one disturbance in Eq. (10). A CLDG matrix element represents the apparent open-loop gain from a disturbance to an output when all control loops are closed in the system. As disturbances should influence controlled outputs as little as possible, all CLDG elements should preferably be small, especially smaller than the control connection frequency response magnitudes "g" of the respective outputs. Unlike the basic RGA, Eqs. (8)–(10) depend on variable scaling and the chosen control connections.

$$\hat{\mathbf{G}}_d(s) = \mathbf{\Gamma}(s) \cdot \bar{\mathbf{G}}_d(s) \quad (10)$$

where $\bar{\mathbf{G}}_d$ is the scaled disturbance transfer function matrix and $\hat{\mathbf{G}}_d$ is the CLDG.

3.3. ICPD optimization

The generic ICPD process optimization problem has been defined in the time domain e.g. by Kookos and Perkins (2004) or Sakizlis et al. (2004). Considering the scope of the CFB steam path optimization problem, these basic formulations can be summarized with Eqs. (11)–(12), which can then be applied to the open-loop steam path model in the Laplace "s" domain.

$$\min_{X,U} J(y(t), u(t), X, U) \quad (11)$$

subject to the process, control and controllability constraints:

$$\begin{cases} m(x'(t), x(t), u(t), X) = 0 \\ m_0(x(0), u(0), X) = 0 \\ \mu(y(t), x(t), u(t)) = 0 \\ n(u'(t), u(t), X, U) \le 0 \\ \varphi(y(t), u(t), U) = 0 \\ \sigma(y(j\omega), u(j\omega), X) = 0 \\ t \epsilon [0, T] \\ \omega \epsilon [0, F] \end{cases} \quad (12)$$

where J is the optimization objective, t is time, T is time range, ω is frequency, F is frequency range, x are process states, u are control variables, X are process parameters, U are controller parameters, m are process equations with initial conditions m_0, n are system inequality constraints, φ are controller equations, y are measurements, μ are measurement equations and σ are controllability equations.

In the steam path ICPD problem, the differential state equations $m(t)$ can be outlined as the state-space representation (Åström and Hägglund, 2006) of the open-loop transfer function models $\mathbf{G}(s)$ and $\mathbf{G}_d(s)$, Eqs. (6)–(7). The states $x(t)$ are the intermediate steam flows and pressures in the steam path (c.f. Fig. A.2). The measurement equations $\mu(t)$ describe how $y(t)$ are obtained from the states, i.e. the main steam pressure $p(t)$ and the turbine steam flow, which is converted by e_E to the electrical power $E(t)$. The inequality constraints $n(t)$ contain gain and rate constraints for $u(t)$ (i.e. $L(t)$ and $v(t)$), as well as bounds for the parameters X and U that are to be optimized. The controller equations comprise the steam pressure and electrical power feedback controllers (PID in this work, Eq. (B.7) transformed to the time domain). Finally, the controllability equations consist of the PRGA and CLDG matrix evaluation in the chosen frequency domain, Eqs. (8)–(10).

The boiler ICPD design must be carried out for the closed-loop steam path in the dynamic domain, where the load-following MW_e setpoint tracking is optimized directly. As can be seen from the process model Eqs. (6)–(7) and (B.1)–(B.6), optimizing any of the process design parameters will directly influence the open-loop system dynamics, as well as the PRGA and CLDG matrices of the system. The process and its controllers also need to be tuned simultaneously within the same framework, as controller tunings would otherwise affect the optimality of process structure alternatives. Moreover, the design requires a large search space especially for the controller parameters.

The ICPD problem can be solved by implementing a hybrid two-level optimization approach. On the upper level, feasible solution regions are first located using a random search algorithm in a wide search space, specified through initial simulations with feasible controller tunings. The regions with the best ICPD objective values are then refined on the lower level, using simplex search optimization. As such, the optimal solution is located in two consecutive stages with two different optimization algorithms, where the closed-loop process response is evaluated for each candidate solution.

As a random search algorithm, the genetic algorithm "ga" of Matlab 2017 (Goldberg, 1989; Conn et al., 1991; Conn et al., 1997) was considered, using a solution population of 500 and 50 maximum generations. In the considered approach, the initial population is randomized, solutions are ranked based on the ICPD objective, and fitness values are obtained as the inverse square root of the rank. 25 solutions with the best fitness values are passed on directly to the next generation as elites, and the remaining generation is formed through crossover and mutation. Parent solutions are selected by organizing the population into segments according to the fitness values and performing the selection at uniform intervals ("stochastic uniform"). Crossover takes place by selecting elements randomly from each parent with a 0.8 crossover fraction. Mutations are calculated by adding a random zero-mean Gaussian vector to a parent ("mutation uniform"), with a mutation probability of 0.15.

The Nelder-Mead simplex search (Lagarias et al., 1998), "fminsearch" in Matlab 2017, was used for the lower level. A simplex of $n+1$ points (n equals the number of parameters) is moved towards the optimum through reflection, expansion, contraction and shrink operations. A constraint modification is used for the design parameters (D'Errico, 2012), utilizing a sinusoid transform

to the unconstrained space. The search is periodically reinitialized by offsetting the optimization parameters one at a time.

In total, the ICPD algorithm can be summarized in the procedure below. While the individual design methods of the boiler ICPD procedure are established in literature, the procedure itself was devised for this paper. Notably, the ICPD optimization is fully simultaneous (Hultgren et al., 2017a) for all continuous parameters of the problem despite its two-level structure: both the upper level random search and lower level simplex search stages optimize the same process and controller parameters, and they use the same objective function to evaluate the results. As the control structure is selected beforehand based on controllability analysis and the process structure is based on design requirements, the discrete design decisions of the boiler steam path were carried out sequentially.

(1) Select the ICPD design parameters and specify the design objective.
(2) Select the 2 × 2 unit master control structure between MVs and CVs (boiler-following or turbine-following) through a PRGA & CLDG analysis in the frequency domain, favoring:
   - control pairings with PRGA elements close to 1
   - small off-diagonal PRGA elements
   - small CLDG elements to minimize the effect of disturbances
(3) Apply the controller equations with feedback (Åström and Hägglund, 2006) to **G**(s), Eq. (6): $p(s)/L(s)$ and $E(s)/v(s)$ for boiler-follow or $p(s)/v(s)$ and $E(s)/L(s)$ for turbine-follow.
(4) Perform initial controller tuning at process parameter limits to locate an approximate feasible region of operation and set it as the ICPD search space.
(5) Perform genetic algorithm optimization for process and controller parameters in the full search space with a limited number of generations.
(6) Construct smaller search space(s) around candidate solution (s) from the genetic algorithm.
(7) Refine solution(s) through simplex search, apply constraints if necessary.
(8) Obtain the ICPD result from the simplex optimization and validate it against a reference case.

4. CFB boiler steam path ICPD

The integrated design setup for the industrial CFB boiler steam path storage capacity, turbine valve throttling trajectory and boiler unit master control structure is discussed here. The control connections between the system CVs (steam pressure, electrical power) and MVs (firing power, turbine valve position) were selected prior to the ICPD optimization in Section 4.1, using PRGA and CLDG analysis. The ICPD algorithm was then implemented to the steam path model in Section 4.2.

4.1. Control structure selection

The PRGA and CLDG were evaluated at ω = 0–0.5 rad/s for Eqs. (6)–(7), using boiler-following and turbine-following control connections. The firing power, turbine valve and DSH disturbance variables were scaled by the distance between their upper and lower saturation limits. For the DSH spray, this was 25% of the main steam flowrate. The main steam pressure and electrical power were scaled by the largest allowed setpoint error: 10% for the power and 20% for the pressure.

The results are displayed in Figs. 4 and 5. At zero frequency, boiler-following diagonal PRGA elements were inferior to turbine-following control because of the small steady-state MW_e gain of the turbine valve. However, boiler-following control became superior already above 0.01 rad/s. In terms of loop interactions, boiler-following control thus provides better load change performance if the firing power is compensated sufficiently at steady-state, which was also discovered by Hultgren et al. (2017b) for plantwide CFB boiler control. The PRGA indicated that at zero frequency, there was a minor off-diagonal interacting effect from the steam pressure control connection. However, it was largely overshadowed by the off-diagonal PRGA element of the electrical power, which increased rapidly above zero frequency, peaked at 0.02 rad/s and diminished slowly after this. The peak is derived from the combined effect of the L and v gains on E. These control performance limiting interactions are thus present for both turbine-following and boiler-following control. Notably, the off-diagonal effects wouldn't have been visible with the dynamic RGA.

The CLDG showed that DSH disturbances will not present control performance issues for the output that is controlled with the turbine valve (output E for boiler-follow mode, steam p for turbine-follow mode), as the corresponding CLDG values were negligible for the entire frequency region. The gain magnitudes of the firing power, on the other hand, were surpassed by their CLDG elements already at 0.02 rad/s, as the firing power response is slow at the turbine. Moreover, below 0.15 rad/s the turbine-following CLDG between E and the DSH spray was much larger than the CLDG between the DSH and p in boiler-follow mode. Thus, steam temperature control action will result in performance problems for the firing power control loop especially in turbine-follow mode.

All in all, the boiler-following structure could be selected for the 2 × 2 boiler system. As this result is supported by design experience for fast load transitions, the boiler-following ICPD results were not benchmarked against similar turbine-following results

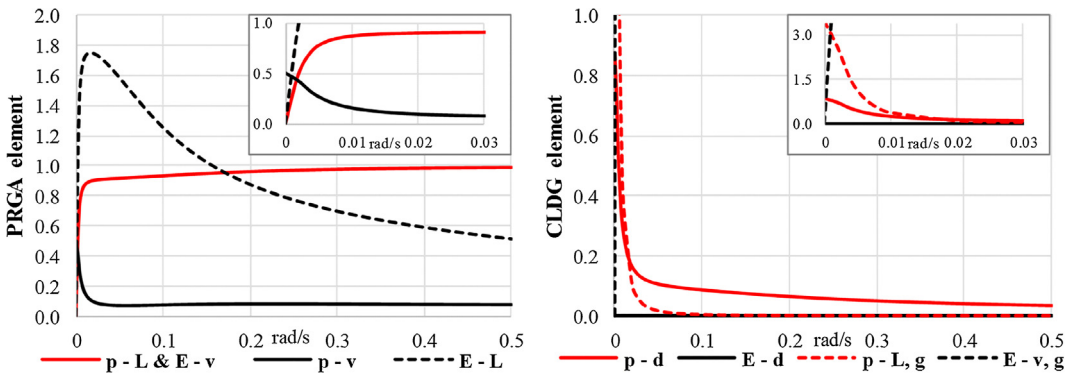

Fig. 4. PRGA magnitudes (left), CLDG and open-loop gain magnitudes (right), for boiler-following control (p control with L, E control with v); steam pressure p, electrical power E, firing power L, turbine valve v, open-loop gain magnitude g. The frequency range 0–0.03 rad/s is magnified.

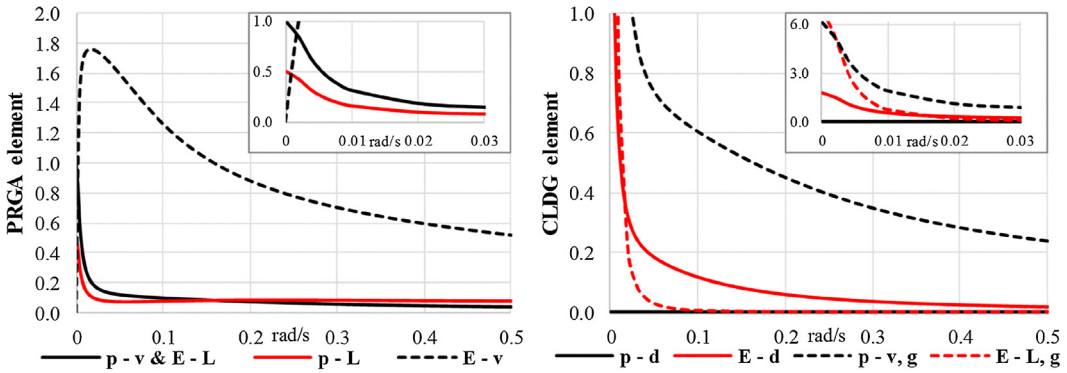

Fig. 5. PRGA magnitudes (left), CLDG and open-loop gain magnitudes (right), for turbine-following control (p control with v, E control with L); steam pressure p, electrical power E, firing power L, turbine valve v, open-loop gain magnitude g. The frequency range 0–0.03 rad/s is magnified.

in this paper. While unit master control is typically implemented using higher-level strategies, multi-loop single-input–single-out put PID control was utilized in this work. The boiler-following closed-loop process model for the optimization was formed from Eq. (6) by applying the PID controller transfer functions, Eq. (B.7), with feedback. Nominal starting values for the PID parameters were obtained through crude tuning with the Matlab 2017 PID tuner (Åström and Hägglund, 2006). These simulations showcased that the derivative action was not necessary for the electrical power PID, and it was thus omitted from further analysis. Challenges in obtaining stable tunings for the boiler-following setup were clearly observed.

4.2. ICPD design setup

Next, the ICPD optimization was performed for the closed-loop boiler model, using boiler-following control. Since the aim was to improve MW_e setpoint tracking during load changes, the optimization was carried out directly in the dynamic domain with different MW_e setpoint ramps. The obtained dynamic responses were assessed based on setpoint tracking and controllability criteria.

4.2.1. Design test matrix

The ICPD optimization was performed separately for four load change scenarios (Table 1). Moderate load change magnitudes of $\leq$15% MW_e were considered in order to remain within a feasible operating region of the linear CFB steam path model. The main focus of the ICPD design was on constant pressure operation, where the electrical power output was ramped to a new load level, while maintaining a constant main steam pressure. Therefore, the main scenarios I and II considered constant pressure operation. Scenario I consisted of a small and fast load change, corresponding to a sudden change in the network load demand. Scenario II was a larger and slower ramp, representing a planned load transition. For comparative purposes, ICPD was also carried out for the same MW_e ramps in sliding-pressure mode in scenarios III and IV: the main steam pressure was ramped together with the electrical power, using the same ramp speed and starting time for both outputs. In a more realistic case, sliding-pressure transitions would require individual ramp programs for the pressure and the output power, but for simplicity this was not considered in this study.

All scenarios were simulated from a stable operating point of 80% output power. The initial load level was chosen in order to investigate turbine valve saturation: Since steam throttling contributes to exergy destruction and should be avoided at nominal loads, the possibility to open the valve enough when load demand increases is limited. For this reason, the ICPD optimization was only carried out for positive load changes. The new setpoint was maintained for 3750 timesteps after each ramp to eliminate the effect of possible oscillations in the analysis.

4.2.2. Target parameters

The parameters to be optimized by the ICPD algorithm are shown in Table 2. The main process parameters were the steam storage capacities of the evaporator (τ_E) and superheating sections 1 (τ_{S1}) and 2 (τ_{S2}), implemented as the total storage τ_{TOT}, the evaporator percentage q_E of this storage, and the percentage q_{S1} of the superheater storage that is placed in τ_{S1}. The turbine valve opening at the 80% load level was included to balance disturbance rejection and exergy destruction. The controller parameters were P, I, D and N for the main steam pressure p, and P and I for the electrical power E.

All process and controller parameters were scaled by dividing them with their nominal starting values. The minimum evaporator storage was limited rather tightly around the design value due to the need to produce a required amount of steam for all process designs. The superheater storage setup could be varied more freely, and a 50% τ_{S1}/τ_{S2} distribution was assumed as the nominal starting value. The turbine valve opening is technically limited between 0 and 100%, but a larger minimum valve opening (0.73 of nominal) was chosen in order to reduce steam throttling. PID parameter boundaries were determined based on the initial controller tuning, observing stability limits and active disturbance rejection, while maintaining the search space as large as possible. While this approach was deemed sufficient for this work, closed-loop stability criteria could be included as a pre-analysis step or as an optimization constraint in a fully systematic boiler ICPD design procedure in the future.

Table 1
Load change test program for the boiler steam path ICPD optimization.

Load change scenario	E setpoint (%)	Ramp time (timesteps)	Ramp speed (% MW/step)	Main steam p setpoint (%)
I: Fast small load ramp at constant p	+5	13	0.385	0
II: Slow large load ramp at constant p	+15	210	0.07	0
III: Fast small load ramp at sliding p	+5	13	0.385	+5
IV: Slow large load ramp at sliding p	+15	210	0.07	+15

Table 2
Parameters to be designed through ICPD. Minimum and maximum constraints reported as multipliers to the nominal starting values of the parameters, i.e. they are normalized.

Process parameter	Name	Min	Max	Controller parameter	Name	Min	Max
Total steam storages	τ_{TOT}	0.42	1.69	Steam p gain, P	P_p	0.00	5.20
Evaporator storage percentage of τ_{TOT}	q_E	0.97	1.25	Steam p integrator, I	I_p	0.01	36944.30
SH storage percentage before DSH of τ_S	q_{S1}	0.20	1.80	Steam p derivator, D	D_p	0.00	12.17
Turbine valve nominal position	$\bar{v}$	0.73	1.22	Steam p D filter, N	N_p	0.00	1991.49
				Output E gain, P	P_E	0.02	114.04
				Output E integrator, I	I_E	0.00	3873.03

4.2.3. Optimization objective

The ICPD optimization objective was constructed as a combination of desirable qualities for the closed-loop load change response, resulting in the weighted sum (13)–(19). The individual terms were scaled by dividing them with their values for the nominal boiler design and control parameters. This approach enabled a direct comparison of conflicting design goals, especially as the starting point for the design was a validated closed-loop process setup. As such, J doesn't have a direct physical significance in the steam path, but rather represents the tradeoff between desirable conflicting design objectives. Weighting factors were selected for the terms j_1–j_6 based on how the cost function terms changed due to typical process parameter modifications.

$$J = j_1 + j_2 + j_3 + j_4 + j_5 + j_6 \tag{13}$$

$$j_1 = \int_0^T (p(t) - p_{SP}(t))^2 dt \tag{14}$$

$$j_2 = 10 \cdot \int_0^T (E(t) - E_{SP}(t))^2 dt \tag{15}$$

$$j_3 = -2 \cdot v(0) \cdot \int_0^T v(t) dt \tag{16}$$

$$j_4 = \int_0^T |v(t) - \max(v(t), v_{min})| dt + \int_0^T |v(t) - \min(v(t), v_{max})| dt \tag{17}$$

$$j_5 = \int_0^F \mathbf{\Gamma}_n(j\omega) d\omega \tag{18}$$

$$j_6 = 2 \cdot \int_0^F \sum \left| \widehat{\mathbf{G}}_d(j\omega) \right| d\omega \tag{19}$$

where J is the ICPD objective, j is an individual design objective, p is pressure, E is electrical power, SP is setpoint, v_{min} and v_{max} are the minimum and maximum boundaries of the turbine valve control signal v, T is the dynamic ramp test duration, F is the investigated frequency range for the relative gain analysis, Γ_n is the PRGA number and $\widehat{\mathbf{G}}_d$ is the CLDG.

Terms j_1 and j_2 account for the main steam pressure and electrical power tracking performance. The performance was evaluated directly by integral square errors for the entire timespan of the load change tests. An equal weight was placed on the load ramp duration and the steady-state period after it. Due to the heavy focus on load change performance, the MW_e error j_2 was given a large weight.

Term j_3 is the turbine valve exergy penalty, which was evaluated by integrating the valve control signal over the test timespan, with an aim to keep the valve open as much as possible. The integral sum was multiplied with the nominal valve position to highlight the initial steady-state. Term j_4 is the valve saturation, calculated by comparing the saturated signal to the unsaturated signal and integrating the difference over time. The purpose of j_4 was to maintain an adequate control reserve for electrical power disturbances.

The effect of input–output controllability was included in terms j_5–j_6, evaluated with the PRGA and the CLDG, which were calculated at ω = 0–0.5 rad/s using the "freqresp" function in Matlab 2017 (Laub, 1981). The goal for controllability j_5 was to minimize the PRGA number, Eq. (9), integrated over frequency range F. The disturbance controllability objective j_6 was to minimize all DSH spray CLDG elements, utilizing a similar absolute sum formulation to Eq. (9). As the CLDG decreased quickly compared to the PRGA at higher frequencies, it was given a slightly larger weight.

5. Results

The outcomes of the boiler steam path ICPD design were analyzed in this section. The design results were compared against load ramps where only the parameters of the main steam pressure and electrical power PID controllers were optimized (all process parameters remained at their original values).

The responses for the constant pressure scenarios can be viewed in Figs. 6–8; the fast 5% ramps (scenario I) in Fig. 6, the slow 15% ramp (scenario II) in Fig. 7. The control signals L and v for both scenarios are depicted in Fig. 8. Process outputs and manipulated variables were normalized with the respective nominal 80% load starting values. The optimized process and controller parameters and the improvements in the ICPD objective are shown in Table 3.

The ICPD algorithm maximized the total steam storage capacity for both ramp scenarios I and II in constant pressure mode. The evaporator storage was minimized, the superheater storage maximized, and the superheater storage was preferably distributed to the section after the DSH spray. The PID parameters were always successfully tuned together with the modified process structure.

The results indicated that adding storage capacity in the whole steam path improved the constant pressure load change performance and controllability. The capacity should be placed close to the turbine to improve the boiler–turbine decoupling and decrease the effect of DSH spray disturbances on the power output. The results thus set a guideline especially for superheater design, as a superheater with a large thermal storage capacity, such as the CFB Intrex™ heat exchanger, should preferably be placed close to the turbine. The results similarly suggested that boilers with small evaporator steam storages, such as once-through boilers, might actually be useful for constant pressure operation.

Results similar to the constant pressure tests were obtained for sliding-pressure load changes (Figs. 9–11). Again, the overall storage capacity was maximized, the evaporator storage was minimized, and the main superheating storage was placed at τ_{S2} (Table 4). The controller parameters were adequately tuned for each modified process.

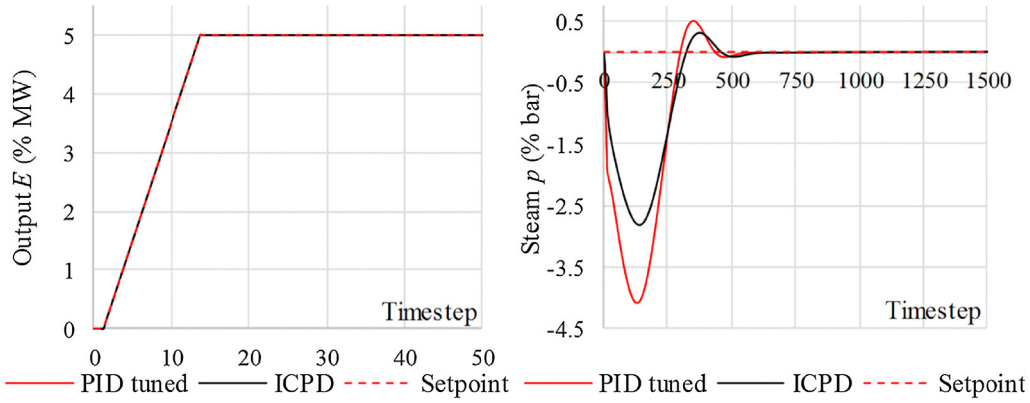

Fig. 6. Normalized electrical power E and main steam pressure p responses during fast 5% constant pressure load ramp (scenario I). Zero level is the nominal starting load.

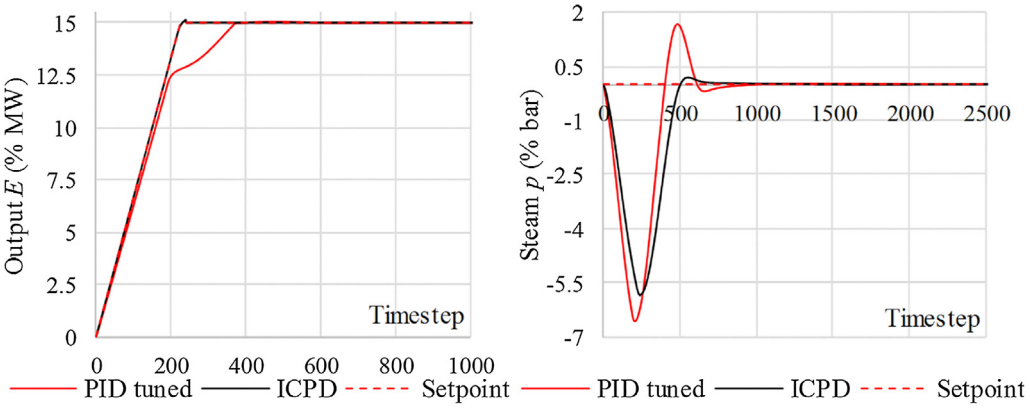

Fig. 7. Normalized electrical power E and main steam pressure p responses during slow 15% constant pressure load ramp (scenario II). Zero level is the nominal starting load.

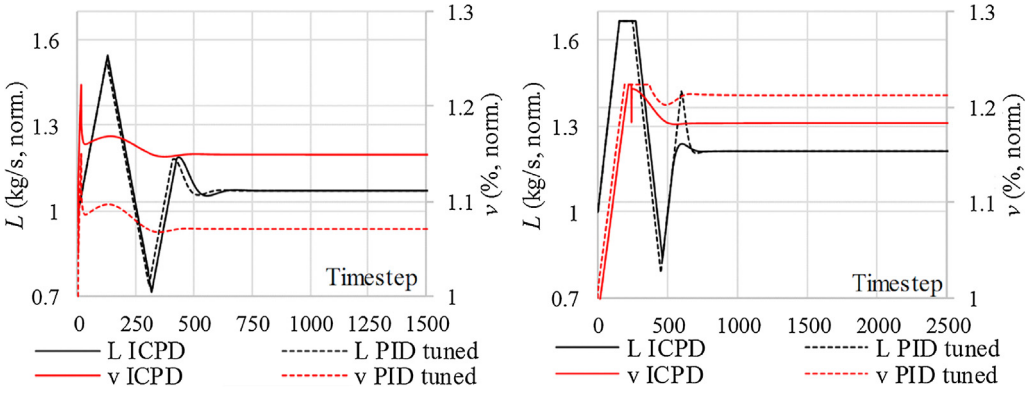

Fig. 8. Firing power (L) and turbine valve (v) during scenarios I (left) and II (right). Both MVs are normalized with their respective starting values, 1 is the nominal MV value.

Table 3
Scenario I and II optimized parameters and objective function values, ICPD and reference PID tuning design cases. Values reported as multipliers to the nominal starting parameters/objectives.

Constant pressure	Parameter, % of nominal value										Objective % of nominal
	τ_{TOT}	q_E	q_{S1}	$\bar{v}$	P_p	I_p	D_p	N_p	P_E	I_E	
ICPD, ramp I	1.69	0.97	0.20	1.08	2.91	2.23	5.09	727.26	2.71	118.88	0.095
PID, ramp I	1	1	1	1	1.85	1.66	3.00	7.41	12.85	3464.13	0.215
ICPD, ramp II	1.69	0.97	0.20	0.97	1.44	2.48	3.70	55.06	2.31	35.58	0.049
PID, ramp II	1	1	1	1	2.00	2.93	3.13	1973.62	0.19	0.002	0.419

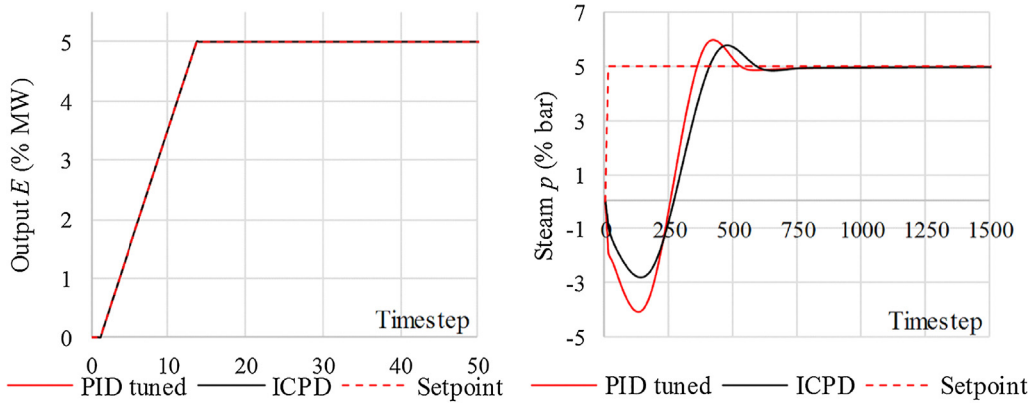

Fig. 9. Normalized electrical power E and main steam pressure p responses during fast 5% sliding-pressure load ramp (scenario III). Zero level is the nominal starting load.

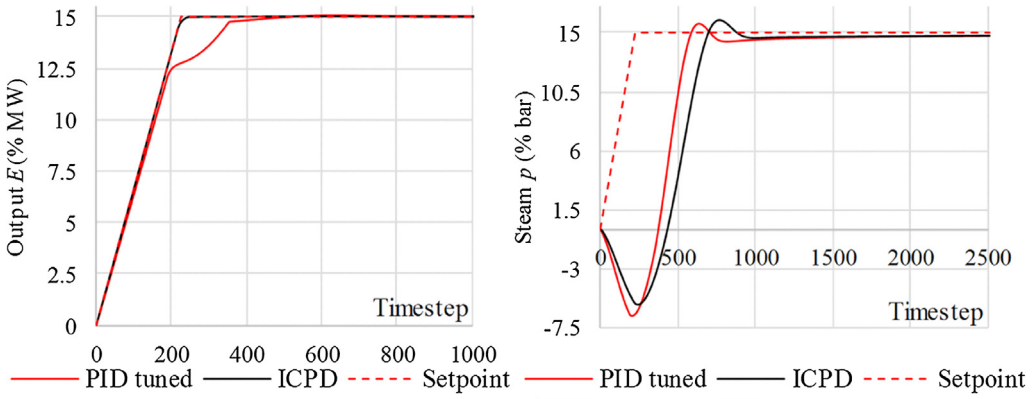

Fig. 10. Normalized electrical power E and main steam pressure p responses during slow 15% sliding-pressure load ramp (scenario IV). Zero level is the nominal starting load.

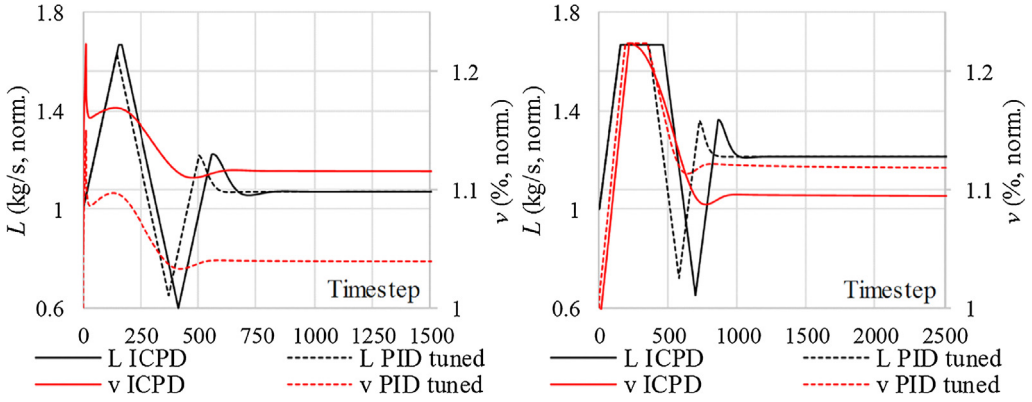

Fig. 11. Firing power (L) and turbine valve (v) during scenarios III (left) and IV (right). Both MVs are normalized with their respective starting values, 1 is the nominal MV value.

Table 4
Scenario III and IV optimized parameters and objective function values, ICPD and reference PID tuning design cases. Values reported as multipliers to the nominal starting parameters/objectives.

Sliding-pressure	Parameter, % of nominal value										Objective % of nominal
	τ_{TOT}	q_E	q_{S1}	$\bar{v}$	P_p	I_p	D_p	N_p	P_E	I_E	
ICPD, ramp III	1.69	0.97	0.20	1.08	1.99	0.56	3.78	11.94	2.87	133.01	0.125
PID, ramp III	1	1	1	1	1.59	0.57	2.80	741.39	12.79	3432.46	0.227
ICPD, ramp IV	1.69	0.97	0.20	0.97	1.64	0.41	3.33	782.93	1.99	0.08	0.088
PID, ramp IV	1	1	1	1	1.31	0.47	2.42	1045.56	0.265	0.001	0.439

Interestingly, the present sliding-pressure results contrasted with the earlier findings of Hultgren et al. (2017a), where only the lumped superheater storage "τ_S" was optimized in sliding-pressure mode together with the boiler-following main steam pressure controller parameters. In that study, the best control performance was obtained with a small superheater storage, and the optimization resulted in improvements in both steam pressure and electrical power control performance.

The differences between the present findings and the previous results can be explained by the nature of boiler-following control. Reaching a new steam pressure setpoint is faster with a small steam storage, while electrical power control benefits from a large storage due to the turbine valve throttle reserve. At the same time, turbine valve MW_e control generates a pressure disturbance, the magnitude of which depends on the steam storage. A large storage thus also has a positive impact on steam pressure control. This tradeoff was confirmed by testing different weighting factors for the objective J. The PRGA and CLDG also favored a large storage, which ultimately lead to the present results.

The turbine valve nominal position was adjusted by the ICPD design for all load scenarios in such a way that load ramps only resulted in short controller saturation periods during the ramp (Figs. 8 and 11). The valve could thus be used effectively for improving load change performance with a minimum exergy penalty. Naturally this behavior depends on the chosen objective function weighting factors. Moreover, similar PID controller parameters were repeated for the different load scenarios, especially for the main steam pressure controller. The largest variations between the ICPD results of different scenarios were seen in the electrical power PID integrator I_E.

All in all, the ICPD design was clearly able to improve the boiler load change performance with simultaneous controller and process design parameter alterations. The hybrid two-level optimization framework was proven to be a robust approach, and the design results could be reproduced reliably during consecutive runs. The objective function breakdown in Table A.1 for the ICPD and optimal PID tuning cases showed that the ICPD results were superior compared to the PID optimization for most individual objectives j_1–j_6. For the fast ramping scenarios I and III, significant improvements in steam pressure tracking and process controllability were obtained at the cost of a negligible electrical power control penalty compared to the optimally tuned PID. For the slow ramps II and IV, the nominal turbine valve position was not enough to obtain the desired setpoint ramp (c.f. Figs. 7 and 10), and the ICPD algorithm thus slightly increased the steam throttling at the 80% starting load.

Despite the successful ICPD implementation, the steam path design case highlighted the challenges of a fully simultaneous dynamic optimization for the entire power plant. Even though the examined boiler and its control structure were simplified (linear mass storage model without other control loops or complex dynamics like the drum water-steam balance), the optimization objective had many local minima especially close to the discovered optima. This problem can be attributed to several reasons. Firstly, a fully simultaneous ICPD approach is inherently multi-optimum in nature, as each set of evaporator and superheater storages essentially has at least one set of preferred controller tunings. Secondly, the ICPD objective was constructed from several conflicting normalized terms. For future work, different objective functions and a more systematic testing of objective weightings could be considered. Thirdly, some of the individual objectives could give similar values for different process and control setups, especially the integral square error terms. This effect was emphasized for the turbine valve–electrical power control loop, as the valve has an immediate MW_e response.

6. Conclusions

Modern power plant design criteria increasingly focus not only on efficiency but also on fast load changes, which requires novel and robust design approaches. Integrated control and process design (ICPD) aims at finding improved plantwide closed-loop process designs through simultaneous optimization of the process and its control system. This work reported, for the first time, the application of an ICPD methodology for the steam path of an industrial circulating fluidized bed boiler in order to obtain improved load change performance.

The goals of the boiler ICPD were to minimize the electrical power (MW_e) tracking error during load changes, maintain adequate main steam pressure control, adjust the turbine valve operation to maintain a sufficient steam control reserve and minimize exergy destruction, and generate process structures with good controllability. To achieve this, an ICPD framework was formulated for a steam storage model of the industrial boiler, utilizing boiler-following control for the electrical power and the main steam pressure. The methodology combines a two-stage dynamic closed-loop optimization with performance relative gain array (PRGA) and closed-loop disturbance gain (CLDG) analysis.

The ICPD design successfully improved the MW_e load changes and the other design goals. For constant pressure mode, the total storage in the steam path was maximized, a maximum storage was placed in the last superheating section, and the evaporator storage was minimized. Tuning of the steam pressure and electrical power controller parameters was provided for the modified process structure. Different load transition scenarios provided similar design outcomes for the process and controller parameters. A large total steam storage was favored by the ICPD algorithm for both constant pressure and sliding-pressure mode, as it enabled quick MW_e changes, good controllability and small pressure disturbances. This is interesting, as boilers with small storage capacities are generally used in sliding-pressure mode.

All in all, the results established an ICPD procedure that can readily be employed for load-following CFB boiler design. The procedure was validated with a linear mass storage modeling approach, describing the steam path as a series of simple dynamic elements. The challenging nature of the optimization problem justified this approach, but more comprehensive results would require detailed modeling, including e.g. combustion side, heat transfer and evaporation dynamics. Economic aspects were not considered at this stage, but they should be included in future work, especially as a large steam storage is a major capital cost for the plant. This could be achieved with an additional economic ICPD design goal or by converting all optimization objectives to their economic counterparts.

The control structure design of this paper considered the performance limiting interactions of main steam pressure and electrical power control, as well as steam temperature control disturbances through the CLDG. In future work, more disturbance scenarios and plantwide control performance will also be evaluated. PID control was exclusively utilized due to its prevalence in power plant control, but future work should also consider advanced model-based control, which has been a growing trend in ICPD literature. This way, the boiler control system could be more closely integrated with the process structure, as the control action would be calculated directly from process modifications, bypassing the need to adjust controller parameters through ICPD. Alternatively, ICPD could employ a two-level embedded approach for process and controller parameters. In any case, the results of this paper stress the importance of a systematic analysis of the power plant control structure and loop interactions in the ICPD design formulation.

Declaration of interests

The authors declared that there is no conflict of interest.

Acknowledgments

The authors would like to acknowledge the industrial-academic cooperation between the University of Oulu and Sumitomo SHI FW Energia Oy (Varkaus, Finland). The work was partly funded by the Graduate School in Chemical Engineering (GSCE) doctoral program (Academy of Finland, Finnish Ministry of Education)

Appendix A

Appendix A contains additional figures and ICPD design results. Fig. A.1 shows example simulations, where the boiler electrical power (controlled variable, CV) is only controlled with the combustion power (fuel + air flows) or the turbine valve (manipulated variables, MV). The results were generated using a transfer function model identified from a full once-through CFB industrial simulator. Rate and gain constraints of the MVs were disregarded in order to highlight the theoretical MV demands during a tightly controlled load change in the electrical power CV.

Fig. A.2 shows the block diagram of the open-loop CFB steam path process model of this paper, complete with transfer function equations for the process blocks.

Table A.1 shows a more detailed objective function evaluation for the ICPD optimization than was given in Tables 3–4, including the values of individual objectives j_1–j_6.

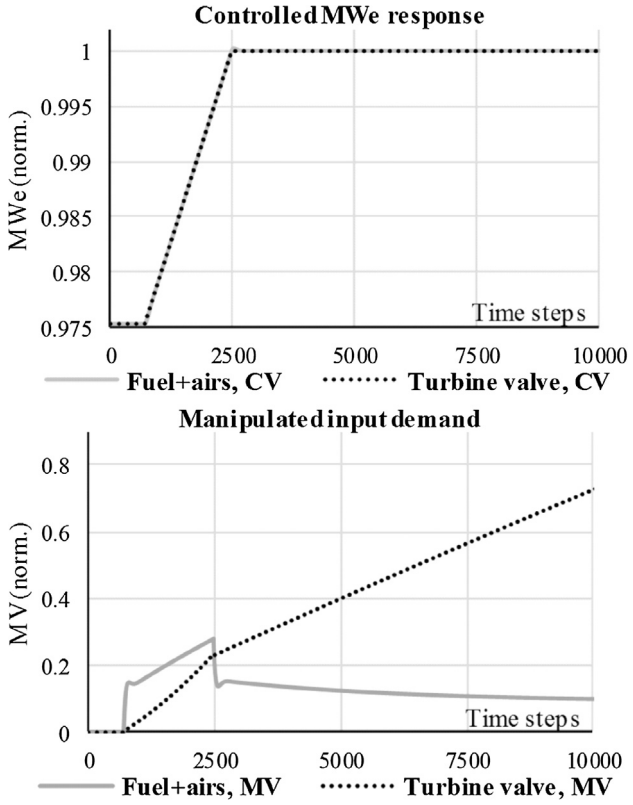

Fig. A1. Manipulated variable demands during a simulated MW_e setpoint ramp, when the output electrical power is only controlled with the turbine valve (dotted) or the fuel + air flows (grey): tight single input–single output PI control, no variable constraints or other control loops active.

Appendix B

Appendix B provides equations for the CFB steam path model transfer function parameters, α, β, γ, δ, ε, ζ, η, θ, κ: The parameters for the process transfer function matrix $\mathbf{G}(s)$, Eq. (6), are given in equation groups (B.1)–(B.4). The parameters for the disturbance transfer function matrix $\mathbf{G}_d(s)$, Eq. (7), are given in equation groups (B.5)–(B.6).

$$\begin{cases} \alpha_{11} = \frac{\rho_W^2}{4f^2\bar{m}_{W,out}^2\tau_I\tau_E\tau_{S1}\tau_{S2}} \\ \beta_{11} = \frac{\rho_W(2\tau_E+\tau_{S1})}{2f\bar{m}_{W,out}\tau_E\tau_{S1}} + \frac{\rho_W}{2f\bar{m}_{W,out}\tau_{S2}} + \frac{r\bar{v}}{\tau_{S2}} + \frac{1}{\tau_I} \\ \gamma_{11} = \frac{\rho_W^2(\tau_E+\tau_{S1}+\tau_{S2})}{4f^2\bar{m}_{W,out}^2\tau_E\tau_{S1}\tau_{S2}} + \frac{r\bar{v}\rho_W(2\tau_E+\tau_{S1})}{2f\bar{m}_{W,out}\tau_E\tau_{S1}\tau_{S2}} + \frac{\rho_W(2\tau_E+\tau_{S1})}{2f\bar{m}_{W,out}\tau_I\tau_E\tau_{S1}} + \frac{\rho_W}{2f\bar{m}_{W,out}\tau_I\tau_{S2}} + \frac{r\bar{v}}{\tau_I\tau_{S2}} \\ \delta_{11} = \frac{\rho_W^2(r\bar{v}\tau_I+\tau_E+\tau_{S1}+\tau_{S2})}{4f^2\bar{m}_{W,out}^2\tau_I\tau_E\tau_{S1}\tau_{S2}} + \frac{r\bar{v}\rho_W(2\tau_E+\tau_{S1})}{2f\bar{m}_{W,out}\tau_I\tau_E\tau_{S1}\tau_{S2}} \\ \varepsilon_{11} = \frac{r\bar{v}\rho_W^2}{4f^2\bar{m}_{W,out}^2\tau_I\tau_E\tau_{S1}\tau_{S2}} \end{cases} \tag{B.1}$$

$$\begin{cases} \alpha_{12} = \frac{\bar{p}r}{\tau_{S2}} \\ \beta_{12} = \frac{\bar{p}r\rho_W(2\tau_E+\tau_{S1})}{2f\bar{m}_{W,out}\tau_E\tau_{S1}\tau_{S2}} \\ \gamma_{12} = \frac{\bar{p}r\rho_W^2}{4f^2\bar{m}_{W,out}^2\tau_E\tau_{S1}\tau_{S2}} \\ \delta_{12} = \frac{\rho_W(2\tau_E+\tau_{S1})}{2f\bar{m}_{W,out}\tau_E\tau_{S1}} + \frac{\rho_W}{2f\bar{m}_{W,out}\tau_{S2}} + \frac{r\bar{v}}{\tau_{S2}} \\ \varepsilon_{12} = \frac{\rho_W^2(\tau_E+\tau_{S1}+\tau_{S2})}{4f^2\bar{m}_{W,out}^2\tau_E\tau_{S1}\tau_{S2}} + \frac{\rho_W r\bar{v}(2\tau_E+\tau_{S1})}{2f\bar{m}_{W,out}\tau_E\tau_{S1}\tau_{S2}} \\ \zeta_{12} = \frac{r\bar{v}\rho_W^2}{4f^2\bar{m}_{W,out}^2\tau_E\tau_{S1}\tau_{S2}} \end{cases} \tag{B.2}$$

$$\begin{cases} \alpha_{21} = \frac{e_E r\bar{v}\rho_W^2(\tau_{HP}+x_{HP}\tau_{LP}-x_{HP}\tau_{HP})}{4f^2\bar{m}_{W,out}^2\tau_I\tau_E\tau_{S1}\tau_{S2}\tau_{HP}\tau_{LP}} \\ \beta_{21} = \frac{e_E r\bar{v}\rho_W^2}{4f^2\bar{m}_{W,out}^2\tau_I\tau_E\tau_{S1}\tau_{S2}\tau_{HP}\tau_{LP}} \\ \gamma_{21} = \beta_{11} + \frac{(\tau_{HP}+\tau_{LP})}{\tau_{HP}\tau_{LP}} \\ \delta_{21} = \gamma_{11} + \frac{(\tau_{HP}+\tau_{LP})}{\tau_{HP}\tau_{LP}}\beta_{11} + \frac{1}{\tau_{HP}\tau_{LP}} \\ \varepsilon_{21} = \delta_{11} + \frac{(\tau_{HP}+\tau_{LP})}{\tau_{HP}\tau_{LP}}\gamma_{11} + \frac{1}{\tau_{HP}\tau_{LP}}\beta_{11} \\ \zeta_{21} = \varepsilon_{11} + \frac{(\tau_{HP}+\tau_{LP})}{\tau_{HP}\tau_{LP}}\delta_{11} + \frac{1}{\tau_{HP}\tau_{LP}}\gamma_{11} \\ \eta_{21} = \frac{(\tau_{HP}+\tau_{LP})}{\tau_{HP}\tau_{LP}}\varepsilon_{11} + \frac{1}{\tau_{HP}\tau_{LP}}\delta_{11} \\ \theta_{21} = \frac{1}{\tau_{HP}\tau_{LP}}\varepsilon_{11} \end{cases} \tag{B.3}$$

$$\begin{cases} \alpha_{22} = \frac{e_E\bar{p}r(\tau_{HP}+x_{HP}\tau_{LP}-x_{HP}\tau_{HP})}{\tau_{HP}\tau_{LP}} \\ \beta_{22} = \frac{e_E\bar{p}r}{\tau_{HP}\tau_{LP}} \cdot \left(\frac{\rho_W(2\tau_E+\tau_{S1})(x_{HP}\tau_{LP}-x_{HP}\tau_{HP}+\tau_{HP})}{2f\bar{m}_{W,out}\tau_E\tau_{S1}} + \frac{\rho_W(x_{HP}\tau_{LP}-x_{HP}\tau_{HP}+\tau_{HP})}{2f\bar{m}_{W,out}\tau_{S2}} + 1 \right) \\ \gamma_{22} = \frac{e_E\bar{p}r}{\tau_{HP}\tau_{LP}} \cdot \left(\frac{\rho_W^2(\tau_E+\tau_{S1}+\tau_{S2})(x_{HP}\tau_{LP}-x_{HP}\tau_{HP}+\tau_{HP})}{4f^2\bar{m}_{W,out}^2\tau_E\tau_{S1}\tau_{S2}} + \frac{\rho_W(2\tau_E+\tau_{S1})}{2f\bar{m}_{W,out}\tau_E\tau_{S1}} + \frac{\rho_W}{2f\bar{m}_{W,out}\tau_{S2}} \right) \\ \delta_{22} = \frac{e_E\bar{p}r}{\tau_{HP}\tau_{LP}} \cdot \frac{\rho_W^2(\tau_E+\tau_{S1}+\tau_{S2})}{4f^2\bar{m}_{W,out}^2\tau_E\tau_{S1}\tau_{S2}} \\ \varepsilon_{22} = \delta_{12} + \frac{(\tau_{HP}+\tau_{LP})}{\tau_{HP}\tau_{LP}} \\ \zeta_{22} = \varepsilon_{12} + \frac{(\tau_{HP}+\tau_{LP})}{\tau_{HP}\tau_{LP}}\delta_{12} + \frac{1}{\tau_{HP}\tau_{LP}} \\ \eta_{22} = \zeta_{12} + \frac{(\tau_{HP}+\tau_{LP})}{\tau_{HP}\tau_{LP}}\varepsilon_{12} + \frac{1}{\tau_{HP}\tau_{LP}}\delta_{12} \\ \theta_{22} = \frac{(\tau_{HP}+\tau_{LP})}{\tau_{HP}\tau_{LP}}\zeta_{12} + \frac{1}{\tau_{HP}\tau_{LP}}\varepsilon_{12} \\ \kappa_{22} = \frac{1}{\tau_{HP}\tau_{LP}}\zeta_{12} \end{cases} \tag{B.4}$$

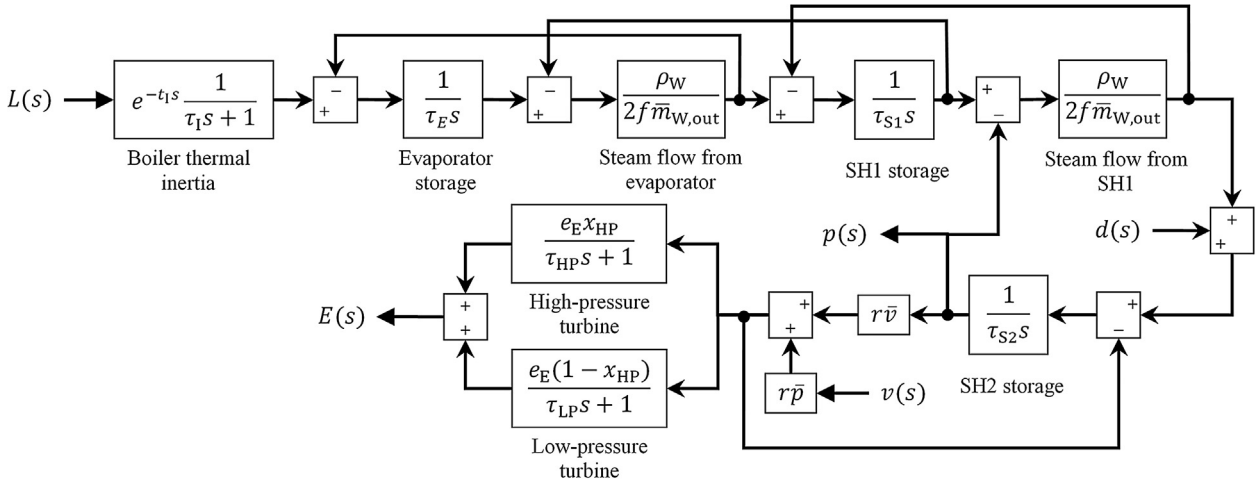

Fig. A2. Transfer function block diagram of the open-loop boiler steam storage capacity model.

Table A.1
Objective function terms j_1–j_6 for all ICPD optimization and PID parameter optimization cases. Results are normalized with the nominal starting objective values (values below 1 signify improvement).

Objective % of nominal	ICPD ramp I	PID ramp I	ICPD ramp II	PID ramp II	ICPD ramp III	PID ramp III	ICPD ramp IV	PID ramp IV
j_1	0.3995	0.7866	0.4686	0.5271	0.8080	0.9536	0.9986	0.8480
j_2	0.0013	0.0000	0.0001	0.3912	0.0012	0.0000	0.0007	0.3865
j_3	1.1563	0.9992	0.9441	0.9956	1.1596	1.0015	0.9602	1.0050
j_4	1.0001	1.00	0.0005	0.0003	1.0001	1.0000	0.0006	0.0041
j_5	0.9978	1	0.9054	1	0.9980	1	0.9082	1
j_6	0.5662	1	0.5730	1	0.5662	1	0.5728	1

$$\begin{cases} \alpha_{d1} = \frac{1}{\tau_{S2}} \\ \beta_{d1} = \frac{\rho_W(2\tau_E+\tau_{S1})}{2f\bar{m}_{W,out}\tau_E\tau_{S1}\tau_{S2}} \\ \gamma_{d1} = \frac{\rho_W^2}{4f^2\bar{m}_{W,out}^2\tau_E\tau_{S1}\tau_{S2}} \\ \delta_{d1} = \delta_{12} \\ \varepsilon_{d1} = \varepsilon_{12} \\ \zeta_{d1} = \zeta_{12} \end{cases} \tag{B.5}$$

$$\begin{cases} \alpha_{d2} = \frac{e_E r\bar{v}(\tau_{HP}+x_{HP}\tau_{LP}-x_{HP}\tau_{HP})}{\tau_{HP}\tau_{LP}\tau_{S2}} \\ \beta_{d2} = \frac{e_E r\bar{v}}{\tau_{HP}\tau_{LP}} \cdot \left(\frac{\rho_W(2\tau_E+\tau_{S1})(\tau_{HP}+x_{HP}\tau_{LP}-x_{HP}\tau_{HP})}{2f\bar{m}_{W,out}\tau_E\tau_{S1}\tau_{S2}} + \frac{1}{\tau_{S2}}\right) \\ \gamma_{d2} = \frac{e_E r\bar{v}}{\tau_{HP}\tau_{LP}} \cdot \left(\frac{\rho_W^2(\tau_{HP}+x_{HP}\tau_{LP}-x_{HP}\tau_{HP})}{4f^2\bar{m}_{W,out}^2\tau_E\tau_{S1}\tau_{S2}} + \frac{\rho_W(2\tau_E+\tau_{S1})}{2f\bar{m}_{W,out}\tau_E\tau_{S1}\tau_{S2}}\right) \\ \delta_{d2} = \frac{e_E r\bar{v}}{\tau_{HP}\tau_{LP}} \cdot \frac{\rho_W^2}{4f^2\bar{m}_{W,out}^2\tau_E\tau_{S1}\tau_{S2}} \\ \varepsilon_{d2} = \varepsilon_{22} \\ \zeta_{d2} = \zeta_{22} \\ \eta_{d2} = \eta_{22} \\ \theta_{d2} = \theta_{22} \\ \kappa_{d2} = \kappa_{22} \end{cases} \tag{B.6}$$

Additionally, Eq. (B.7) shows the standard form of the PID controller with derivative filtering, modified from Åström and Hägglund (2006). The P, I and D parameters are referred to for the pressure and electrical power feedback controllers in Table 2.

$$C(s) = P + I \cdot \frac{1}{s} + D \cdot \frac{N}{s+N} \tag{B.7}$$

References

Alobaid, F., Mertens, N., Starkloff, R., Lanz, T., Heinze, C., Epple, B., 2016. Progress in dynamic simulation of thermal power plants. Prog. Energy Combust. Sci. 59, 79–162.

Aurora, C., Magni, L., Scattolini, R., Colombo, P., Pretolani, F., Villa, G., 2004. Predictive control of thermal Power Plants. Int. J. Robust Nonlin. Control. 14 (4), 415–433.

Bristol, E.H., 1966. On a new measure of interaction for multivariable process control. IEEE Trans. Autom. Control. 11 (1), 133–134.

Capra, F., Martelli, E., 2015. Numerical optimization of combined heat and power Organic Rankine Cycles – Part B: Simultaneous design & part-load optimization. Energy 90 (1), 329–343.

Chan, K.H., Dozal-Mejorada, E.J., Cheng, X., Kephart, R., Ydstie, B.E., 2014. Predictive control with adaptive model maintenance: Application to power plants. Comput. Chem. Eng. 70, 91–103.

Chen, C., Bollas, G.M., 2017. Semi-batch chemical-looping reactors integrated with combined cycle power plants operating at transient electricity demand. In: Proceedings of the FOCAPO/CPC 2017 Conference, Tucson, January 8–12, 2017. FOCAPO/CPC, Tucson, AR, 6 p.

Conn, A.R., Gould, N.I.M., Toint, P.L., 1991. A globally convergent augmented lagrangian algorithm for optimization with general constraints and simple bounds. SIAM J. Numer. Anal. 28 (2), 545–572.

Conn, A.R., Gould, N.I.M., Toint, P.L., 1997. A globally convergent augmented lagrangian barrier algorithm for optimization with general inequality constraints and simple bounds. Math. Comput. 66 (217), 261–288.

D'Errico, J., 2012. fminsearchbnd, fminsearchcon, Mathworks, Mathworks File Exchange. Online: https://www.mathworks.com/matlabcentral/fileexchange/8277-fminsearchbnd–fminsearchcon (accessed 12.05.18).

Diangelakis, N.A., Burnak, B., Pistikopoulos, E.N., 2017. A multi-parametric programming approach for the simultaneous process scheduling and control – Application to a domestic cogeneration unit. In: Proceedings of the FOCAPO/CPC 2017 Conference, Tucson, January 8–12, 2017. FOCAPO/CPC, Tucson, AR, 6 p.

Diangelakis, N.A., Pistikopoulos, E.N., 2016. Modelling, design and control optimization of a residential scale CHP system. In: Kopanos, G.M., Liu, P., Georgiadis, M.C. (Eds.), Advances in Energy Systems Engineering. Springer, Cham, Switzerland, pp. 475–506.

Diangelakis, N.A., Pistikopoulos, E.N., 2017. A multi-scale energy systems engineering approach to residential combined heat and power systems. Comput. Chem. Eng. 102, 128–138.

Doležal, R., Varcop, L., 1970. Process Dynamics, Automatic Control of Steam Generation Plant. Elsevier, Amsterdam, Netherlands.
Franzosi, R., Miotti, A., Pretolani, F., Scattolini, R., 2006. Traditional and advanced control of coal power plants: a comparative study. In: Proceedings of the American Control Conference, Minneapolis, June 14–16, 2006. IEEE, Minneapolis, MN, pp. 3451–3456.
Garduno-Ramirez, R., Lee, K.Y., 2005. Compensation of control-loop interaction for power plant wide-range operation. Control Eng. Pract. 13 (12), 1475–1487.
Garrido, J., Morilla, F., Vázquez, F., 2009. Centralized PID control by decoupling of a boiler-turbine unit. In: Proceedings of the European Control Conference, Budapest, August 23–26, 2009. EUCA, Budapest, Hungary, pp. 4007–4012.
Goldberg, D.E., 1989. Genetic Algorithms in Search, Optimization & Machine Learning. Addison-Wesley, Boston, MA.
Hultgren, M., Ikonen, E., Kovács, J., 2017a. Integrated control and process design in CFB boiler design and control – application possibilities. In: Dochain, D., Henrion, D., Peaucelle, D. (Eds.), Proceedings of the 20th IFAC World Congress, Toulouse, July 9–14, 2017. IFAC, Toulouse, France, pp. 1997–2004.
Hultgren, M., Ikonen, E., Kovács, J., 2017b. Once-through circulating fluidized bed boiler control design with the dynamic relative gain array and partial relative gain. Ind. Eng. Chem. Res. 56 (48), 14290–14303.
Hultgren, M., Kovács, J., Ikonen, E., 2015. Combustion control in oxy-fired circulating fluidized bed combustion. In: Proceedings of the 22nd International Conference on Fluidized Bed Conversion, Turku, June 14–17, 2015. FBC, Turku, Finland, pp. 1195–1205.
IEA, 2011. Harnessing Variable Renewables, A Guide to the Balancing Challenge. International Energy Agency, Paris, France.
Jin, B., Su, M., Zhao, H., Zheng, C., 2015. Plantwide control and operating strategy for air separation unit in oxy-combustion power plants. Energy Conv. Manage. 106, 782–792.
Joronen, T., Kovács, J., Majanne, Y., 2007. Voimalaitosautomaatio. Suomen Automaatioseura ry, Helsinki, Finland.
Klaučo, M., Kvasnica, M., 2017. Control of a boiler-turbine unit using MPC-based reference governors. Appl. Therm. Eng. 110, 1437–1447.
Klefenz, G., 1986. Automatic Control of Steam Power Plants. B.I.-Wissenschaftsverlag, Mannheim/Wien/Zürich, Germany/Austria/Switzerland.
Kong, X., Liu, X., Lee, K.Y., 2015. Nonlinear multivariable hierarchical model predictive control for boiler-turbine system. Energy 93 (1), 309–322.
Kookos, I.K., Perkins, J.D., 2004. The back-off approach to simultaneous design and control. In: Seferlis, P., Georgiadis, M.C. (Eds.), The Integration of Process Design and Control. Elsevier, Amsterdam, Netherlands, pp. 216–238.
Kovács, J., Kettunen, A., Ojala, J., 2012. Modelling and control design of once-through boilers. In: Fadel, M., Caux, S. (Eds.), Proceedings of the 8th Power Plant & Power System Control Symposium, Toulouse, September 2–5, 2012. IFAC, Toulouse, France, pp. 196–200.
Kundur, P., 1994. Power System Stability and Control. McGraw-Hill, USA.
Lagarias, J.C., Reeds, J.A., Wright, M.H., Wright, P.E., 1998. Convergence properties of the Nelder-mead simplex method in low dimensions. SIAM J. Optim. 9 (1), 112–147.
Laub, A.J., 1981. Efficient multivariable frequency response computations. IEEE Trans. Autom. Control. 26 (2), 407–408.
Ławryńczuk, M., 2017. Nonlinear predictive control of a boiler-turbine unit: A state-space approach with successive on-line model linearisation and quadratic optimisation. ISA Trans. 67, 476–495.
Liu, X., Guan, P., Chan, C.W., 2010. Nonlinear multivariable power plant coordinate control by constrained predictive scheme. IEEE Trans. Control Syst. Tech. 18 (5), 1116–1125.
Long, D., Wang, W., Yao, C., Liu, J., 2017. An experiment-based model of condensate throttling and its utilization in load control of 1000 MW power units. Energy 133, 941–954.
Ma, L., Lee, K.Y., Wang, Z., 2016. Intelligent coordinated controller design for a 600 MW supercritical boiler unit based on expanded-structure neural network inverse models. Control Eng. Pract. 53, 194–201.
McAvoy, T.J., 1983. Some results on dynamic interaction analysis of complex control systems. Ind. Eng. Chem. Proc. Des. Dev. 22 (1), 42–49.
Niva, L., Hultgren, M., Ikonen, E., Kovács, J., 2017. Control structure design for oxy-fired circulating fluidized bed boilers using self-optimizing control and partial relative gain analyses. In: Dochain, D., Henrion, D., Peaucelle, D. (Eds.), Proceedings of the 20th IFAC World Congress, Toulouse, July 9–14, 2017. IFAC, Toulouse, France, pp. 2023–2030.
Niva, L., Ikonen, E., Kovács, J., 2015. Self-optimizing control structure design in oxy-fuel circulating fluidized bed combustion. Int. J. Greenhouse Gas Control 43, 93–107.
Ogunnaike, B.A., Ray, W.H., 1994. Process Dynamics, Modeling, and Control. Oxford University Press, New York, NY.
Prasad, G., Irwin, G.W., Swidenbank, E., Hogg, B.W., 2000. Plant-wide predictive control for a thermal power plant based on a physical plant model. IEE Proc. Control Theory Appl. 147 (5), 523–537.
Prasad, G., Irwin, G.W., Swidenbank, E., Hogg, B.W., 2002. A hierarchical physical model-based approach to predictive control of a thermal power plant for efficient plant-wide disturbance rejection. Trans. Inst. Meas. Control 24 (2), 107–128.
Rovnak, J.A., Corlis, R., 1991. Dynamic matrix based control of fossil power plants. IEEE Trans. Energy Conv. 6 (2), 320–326.
Sakizlis, V., Perkins, J.D., Pistikopoulos, E.N., 2004. Recent advances in optimization-based simultaneous process and control design. Comput. Chem. Eng. 28 (10), 2069–2086.
Sarkar, D.K., 2015. Thermal Power Plant Design and Operation. Elsevier, Amsterdam, Netherlands.
Sharifzadeh, M., 2013. Integration of process design and control: A review. Chem. Eng. Res. Des. 91 (12), 2515–2549.
Skogestad, S., Postlethwaite, I., 2005. Multivariable Feedback Control, Analysis and Design. Wiley, Chichester, U.K.
Vega, P., Lamanna de Rocco, R., Revollar, S., Francisco, M., 2014. Integrated design and control of chemical processes – Part I: Revision and classification. Comput. Chem. Eng. 71, 602–617.
Wang, W., Li, L., Long, D., Liu, J., Zeng, D., Cui, C., 2017. Improved boiler-turbine coordinated control of 1000 MW power units by introducing condensate throttling. J. Proc. Control. 50, 11–18.
Wang, W., Liu, J., Zeng, D., Niu, Y., Cui, C., 2015. An improved coordinated control strategy for boiler-turbine units supplemented by cold source flow adjustment. Energy 88, 927–934.
Wang, W., Zeng, D., Liu, J., Niu, Y., Cui, C., 2014. Feasibility analysis of changing turbine load in power plants using continuous condenser pressure adjustment. Energy 64, 533–540.
Witcher, M.F., McAvoy, T.J., 1977. Interacting control systems: Steady state and dynamic measurement of interaction. ISA Trans. 16, 35–41.
Yuan, Z., Chen, B., Sin, G., Gani, R., 2012. State-of-the-art and progress in the optimization-based simultaneous design and control for chemical processes. AIChE J. 58 (6), 1640–1659.
Zhang, S., Taft, C.W., Bentsman, J., Hussey, A., Petrus, B., 2012. Simultaneous gains tuning in boiler/turbine PID-based controller clusters using iterative feedback tuning methodology. ISA Trans. 51 (5), 609–621.
Zhang, F., Wu, X., Shen, J., 2017. Extended state observer based fuzzy model predictive control for ultra-supercritical boiler-turbine unit. Appl. Therm. Eng. 118, 90–100.
Zhou, Y., Wang, D., 2017. An improved coordinated control technology for coal-fired boiler-turbine plant based on flexible steam extraction system. Appl. Therm. Eng. 125, 1047–1060.
Åström, K.J., Hägglund, T., 2006. Advanced PID Control. ISA – Instrumentation, Systems, and Automation Society. Research Triangle Park, NC.